Final accepted version of: Lucke, M., Chioua, M., Grimholt, C., Hollender, M., Thornhill, N.F., 2020, Integration of alarm design in fault detection and diagnosis through alarm-range normalization Control Engineering Practice, 98, 104388, https://doi.org/10.1016/j.conengprac.2020.104388

Integration of alarm design in fault detection and diagnosis through alarm-range normalization ⋆

Matthieu Lucke[a,b,*], Moncef Chioua[a], Chriss Grimholt[c], Martin Hollender[a], Nina F. Thornhill[b]

[a] *ABB Corporate Research Germany, Wallstadter Strasse 59, 68526 Ladenburg, Germany*
[b] *Centre for Process Systems Engineering, Department of Chemical Engineering, Imperial College London, London SW7 2AZ, UK*
[c] *ABB Energy Industries, Ole Deviks Vei 10, 0666 Oslo, Norway*

Abstract

Alarm systems designed according to engineering and safety considerations provide the primary source of information for operators when it comes to abnormal situations. Still, alarm systems have rarely been exploited for fault detection and diagnosis. Recent work has demonstrated the benefits of alarm logs for fault detection and diagnosis. However, alarm settings conceived during the alarm design stage can also be integrated into fault detection and diagnosis methods. This paper suggests the use of those alarm settings in the preprocessing of the process measurements, proposing a normalization based on the alarm thresholds of each process variable. Normalization is needed to render process measurements dimensionless for multivariate analysis. While common normalization approaches such as standardization depend on the historical process measurements available, the proposed alarm-range normalization is based on acceptable variations of the process measurements. An industrial case study of an offshore oil gas separation plant is used to demonstrate that the alarm-range normalization improves the robustness of popular methods for fault detection, fault isolation, and fault identification.

Keywords: Alarm systems, Fault detection and diagnosis.

⋆This project has received funding from the European Union's Horizon 2020 research and innovation programme under the Marie Skłodowska-Curie grant agreement No 675215.
*Corresponding author
Email address: matthieu.lucke@de.abb.com (Matthieu Lucke)

1. Introduction

Alarm management and Fault Detection and Diagnosis (FDD) are two disciplines that are closely related but still separated in the industry. Alarm management corresponds to a collection of processes and practices for determining, documenting, designing, operating, monitoring, and maintaining alarm systems (IEC, 2014). It belongs to the sphere of process safety with established practices (Hollifield and Habibi, 2011) and standards (IEC, 2014). The alarm lifecycle can be divided into three stages (Wang et al., 2016): alarm configuration, alarm design, and alarm removal. Alarm configuration deals with the selection of process variables to be configured with alarms and the determination of alarm priorities. Alarm design corresponds to the design (or redesign) of the alarm generation mechanism that transforms process variables into alarms. Alarm removal aims at limiting of consequential alarms due to the propagation of abnormal situations. In the following, an alarm log refers to the record of alarms generated during the operation of the plant, and the alarm settings indicate the meta-information available for each type of alarm such as the associated process measurement and the parameters of the alarm generation mechanism.

In contrast to alarm management, FDD has emerged from the process control community as a support tool for abnormal situation management. Fault detection consists in determining whether a fault happened and fault diagnosis consists in determining which fault happened through fault isolation (i.e. finding the process process variables affected by the fault) or fault identification (i.e. identifying the type of fault that occurred) (Ge et al., 2013). This paper examines data-driven FDD methods, which are traditionally based on process measurements that correspond to the measurements of the physical quantities (i.e. the process variables) from the industrial process.

Process measurements are key elements in alarm management, in particular for applications such as alarm design (Wang et al., 2016), but FDD applications taking alarm logs into account are limited. Alarm logs were used for purposes

related to FDD such as online alarm flood classification for operator support, but independently from the process measurements (Lucke et al., 2019a). Several works (Rodrigo et al., 2016; Hu et al., 2017a) demonstrated the benefits of a preliminary analysis of alarm logs before carrying the root cause analysis on the process measurements. Bayesian fusion (Stief et al., 2018) was used to improve online fault detection and identification by combining process measurements and alarm logs.

Availability and quality of process measurements are major obstacles to successful implementation of data-driven FDD methods in the industry. Preprocessing is a prerequisite for applying those methods on industrial process measurements, and normalization is a key element of preprocessing (Ge et al., 2017). Normalization is usually based on statistical indicators inferred from the process measurements used for training the FDD methods, but limited availability of process measurements also impact the normalization. The significance of the variations of the process measurements may be difficult to infer from historical data alone. Conversely, finding historical datasets with significant variations of all process measurements is a difficult and time-consuming task for FDD engineers.

This paper investigates an alternative normalization based on the preliminary work in Lucke et al. (2018a) that relies on the alarm settings defined during the alarm design stage. The proposed Alarm-Range (AR) normalization uses the difference between the low and the high alarm thresholds for each process variable to place the variations of the related process measurement in the context of the safe operational range. AR-normalization does not depend on the choice of the training data, which has two benefits: it facilitates the work of FDD engineers by removing constraints on the variability of the measurements in the choice of the training data, and it limits spurious FDD results due to the use of miscalibrated statistical indicators in the normalization.

While the preliminary work by Lucke et al. (2018a) focused on demonstrating the advantage of AR-normalization on a simple case for fault identification, this paper provides a more advanced study of the effect of AR-normalization on fault

detection, fault isolation, and fault identification on reference methods in the industry, namely Principal Component Analysis (PCA) for fault detection and fault isolation, and nearest neighbour classification for fault identification. The analysis is carried on an industrial case study of an offshore oil gas separation plant.

Section 2 gives additional information about alarm design and the integration of alarm systems in FDD and also reviews normalization practices. Section 3 discusses the motivation for a new normalization approach that does not rely on statistical indicators. Section 4 details the normalization, the fault detection, isolation, and identification methods used for the analysis. Section 5 introduces the oil gas separation plant as a representative industrial case study that can be used to demonstrate the benefits of AR-normalization. The results of the study are presented and discussed in Section 6.

2. Background

2.1. Alarm design

An alarm is an audible or visible means of indicating to the operator an equipment malfunction, process deviation, or abnormal condition requiring a timely response (IEC, 2014). Various types of alarms can be defined during the alarm design stage corresponding to various alarm generation mechanisms (IEC, 2014). Absolute alarms for example are generated when an alarm threshold is exceeded.

The choice of the alarm generation mechanism and the corresponding parameters are examples of alarm settings. Alarm settings are conceived during the engineering stage of the plant based on safety and technical considerations. Figure 1 illustrates the alarm design procedure for absolute alarms and their alarm thresholds. The consequence threshold is first defined as the limit after which a consequence begins to occur (e.g. for the level of a tank, it could be the maximum level the tank can admit before overflow). The alarm threshold is defined from the consequence threshold taking into account the process deadtime,

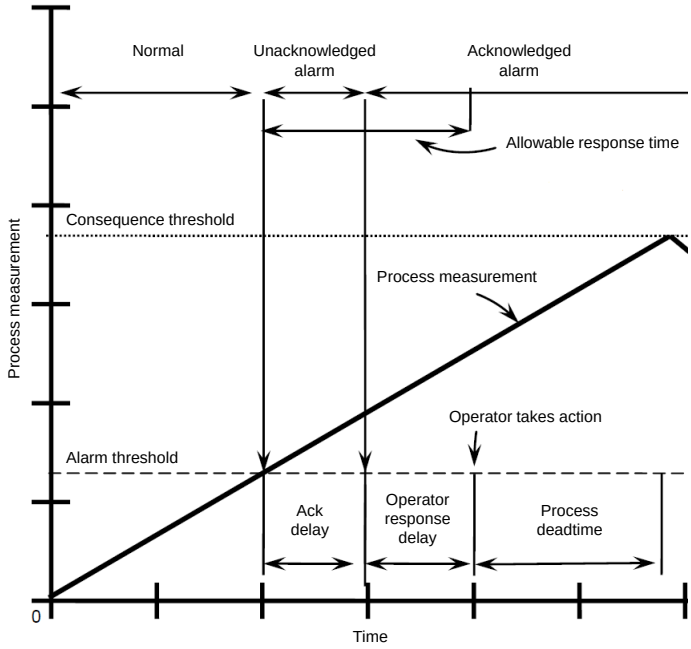

Figure 1: Alarm response timeline adapted from IEC (2014).

the operator response delay and the acknowledgement delay for the corresponding process measurement. A high and a low alarm threshold are usually defined for each process variable.

This paper focuses on absolute alarms and their alarm thresholds for use in preprocessing measurements for FDD.

2.2. Integrating alarm systems in fault detection and diagnosis

Alarms are the foremost indicators for operators when it comes to detecting and identifying ongoing abnormal situations on the plant. Improving alarm management based on analysis of the process measurements is a common research direction (Wang et al., 2016). Several methods have been proposed to design the best alarm thresholds based on process measurements using a univariate approach (Xu et al., 2012) or a multivariate approach (Yang and Guo, 2017). Alarm configuration and alarms triggered by abnormality propagation

are other problems for which solutions based on the analysis of process measurements have been proposed (Wang et al., 2016).

Methods for analysis of alarm logs can help investigating abnormal situations (Lucke et al., 2019a) such as alarm floods, conditions during which the alarm rate is greater than the operator can effectively manage (IEC, 2014). Online alarm flood classification methods (Charbonnier et al., 2015, 2016; Lai et al., 2017; Lucke et al., 2018b; Dorgo et al., 2018) rely on approaches that are close to traditional fault detection and identification approaches (Lucke et al., 2019a), but only consider alarm logs.

Preliminary analysis of alarm logs can be applied to speed up root cause analysis based on process measurements. Rodrigo et al. (2016) clustered similar abnormal situations based on their alarms before proceeding to root cause analysis on process measurements. Hu et al. (2017a) conducted a preliminary root cause analysis on alarm logs to identify process variables that could be root cause candidates and reduce the scope of root cause analysis on process measurements .

Statistical alarms are a particular case since they are generated using statistical indicators of the process measurements such as the standard deviation in fault-free operation. Statistical alarms can be substituted for process measurements to reduce the computational load, in particular for root cause analysis with transfer entropy (Yu and Yang, 2015; Su et al., 2017; Hu et al., 2017b). Statistical alarms can also be substituted for process measurements when doing variable selection for fault detection and identification to limit the impact of noisy variations of the process measurements (Lucke et al., 2019b).

Direct integration of process measurements and alarm logs for fault detection and identification has been addressed in Stief et al. (2018) where a two-stage Bayesian classifier is used. Stief et al. (2019) have released a dataset from a multiphase flow rig to underpin future research into the integration of heterogeneous data for fault detection and identification, in particular alarm logs and process measurements.

2.3. Normalization of process measurements

2.3.1. Common practices in fault detection and diagnosis

FDD on a process plant is traditionally based on the process measurements corresponding to process variables X_m measured at each sampling time t_n, where $m = 1, \ldots, M$ and M is the total number of process variables considered. $x_m(t_n)$ indicates the value of X_m measured at t_n. The plant vector $\mathbf{X}$ is defined as the M-dimensional variable taking values $\mathbf{x}(t_n) = [x_1(t_n), x_2(t_n), \ \ldots \ , x_M(t_n)]^T$ at time t_n. This paper investigates the effect of normalization on sample-wise FDD methods that rely on the values of the plant vector at each sampling time t_n. The effect of normalization on FDD methods using sliding windows (Shang et al., 2017a) or taking into account autocorrelation in the process measurements would require a separate analysis, since autocorrelation of process measurements is an important factor for monitoring of industrial processes under feedback control.

Process measurements associated with the variables X_m have various engineering units and scales and may need to be preprocessed so that they are dimensionless, to match the requirements of online FDD methods (Ge et al., 2017). Normalization is generally based on the statistical properties of the process measurements used for training the method. The training set can contain process measurements from normal operation (in this case it is named $\check{\Omega}_{N0}$) or process measurements from faulty operation (i.e. $\check{\Omega}_F$). The process measurements in the test set Ω_{N_0} are normalized using the statistics of the training set $\check{\Omega}_{N0}$ and the process measurements in the test set Ω_F are normalized using the statistics of the training set $\check{\Omega}_F$.

Methods for fault detection and fault isolation are usually trained on $\check{\Omega}_{N0}$ in order to assess how abnormal a new measurement is. In this case, centering and scaling of the variance of the process measurements using the mean and standard deviation of $\check{\Omega}_{N0}$ is a common approach.

Methods for fault identification are usually trained on $\check{\Omega}_F$ to recognize the selected types of faults, but normalization practices vary. Mean-centering of the

process measurements is a pre-requisite for many methods but scaling might not be necessary since not all methods require dimensionless measurements. In particular, fault identification methods using features learnt from the training data (such as methods based on deep learning (Zhang and Zhao, 2017; Wu and Zhao, 2018)) have been used without scaling the process measurements. When dimensionless measurements should be used, standardization can be based on the statistics of $\check{\Omega}_F$ but can also be based on the statistics of $\check{\Omega}_{N0}$, in particular if the fault identification method is directly based on the output of fault detection method. In this case, the normalization statistics are the same as the ones used for fault detection, e.g. the mean and the standard deviation of $\check{\Omega}_{N0}$ (Tong and Palazoglu, 2016; Zhu and Song, 2010; Gajjar and Palazoglu, 2016).

Other approaches exist but remain rare. Shu and Zhao (2016) used feature scaling where the extrema of the process measurements in $\check{\Omega}_{N0}$ are used to scale the process measurements between zero and one. Vargas et al. (2017) divided the mean-centered process measurement by the mean of the process measurements in $\check{\Omega}_{N0}$, and Shang et al. (2017b) divided the process measurements by the range (i.e. the difference between the maximum and minimum) of the process measurements in $\check{\Omega}_{N0}$.

2.3.2. Selected normalization for fault detection and isolation

The most common normalization approach for fault detection and isolation is standardization using $\check{\Omega}_{N0}$ statistics from normal operation, which is referred to as N-standardization in the rest of the paper. The N-standardized plant vector at time t_n is defined as $\tilde{\mathbf{x}}(t_n) = [\tilde{x}_1(t_n), \ \dots \ , \tilde{x}_M(t_n)]^T$ where:

$$\tilde{x}_m(t_n) = \frac{x_m(t_n) - \mu_m(\check{\Omega}_{N0})}{\sigma_m(\check{\Omega}_{N0})} \tag{1}$$

where $\mu_m(\check{\Omega}_{N0})$ and $\sigma_m(\check{\Omega}_{N0})$ are respectively the mean and standard deviation of process variable X_m in $\check{\Omega}_{N0}$.

2.3.3. Selected normalization for fault identification

For fault identification, the most common normalization approach is F-standardization, which corresponds to a standardization using the standard

deviation in faulty operation. The F-standardized plant vector at time t_n is defined as $\tilde{\mathbf{x}}(t_n) = [\tilde{x}_1(t_n), \ \ldots \ , \tilde{x}_M(t_n)]^T$ where:

$$\tilde{x}_m(t_n) = \frac{x_m(t_n) - \mu_m(\check{\Omega}_{N0})}{\sigma_m(\check{\Omega}_F)} \tag{2}$$

where $\mu_m(\check{\Omega}_{N0})$ is the mean of process variable X_m in $\check{\Omega}_{N0}$ and $\sigma_m(\check{\Omega}_F)$ is the standard deviation of process variable X_m in $\check{\Omega}_F$.

3. Motivation for the method

Normalization can have a high impact on the performance of FDD methods. Existing normalization approaches such as standardization are dependent on the availability of historical process measurements to estimate appropriate statistical indicators (e.g. standard deviation) for each process measurement. In practice, finding normal operation data $\check{\Omega}_{N0}$ or faulty data $\check{\Omega}_F$ that can be used for training the FDD model is a difficult and time-consuming task.

For $\check{\Omega}_{N0}$, it is challenging to find a time interval where all process measurements are fault-free and where all process measurements present representative variations. Variations during the fault-free interval do not necessarily give a good indication of the acceptable range of variations of the process measurements. For example, variations of process measurements under feedback control are usually small and may not provide robust statistical indicators for the normalization, e.g. for N-standardization. Sub-section 5.1 gives an example of industrial case study where the process measurements present a low variability during normal operation. The case study considers the water reinjection section of an offshore oil gas separation plant where the water flows are controlled to ensure the safe operation of the plant. Sub-sections 6.2 and 6.3 show how traditional N-standardization combined with the low variability of the measurements in $\check{\Omega}_{N0}$ can lead to spurious results in fault detection and fault isolation.

F-standardization also depends on the faulty process measurements available for training in $\check{\Omega}_F$. The patterns of the process measurements during fault occurrences in the training set might not be exactly the same as the patterns

of the process measurements in new occurrences, and a change in amplitude of variation of a measurement from the training set to the test set can be amplified by the standardization. Sub-section 6.4 illustrates how F-standardization combined with changing fault characteristics can lead to spurious fault identification.

The proposed AR-normalization is intended as a normalization approach that should facilitate and speed up the work of the engineers in charge of implementing FDD methods in industrial environments. AR-normalization scales process measurements using the alarm range (the difference between the upper and lower alarm thresholds). Such scaling is independent of the statistics of the training data and can be used both for fault detection and isolation and for fault identification. Therefore, the engineers do not need to consider the variability of the measurements in the choice of the training data and can focus on isolating the intervals of normal operation and the fault intervals for $\check{\Omega}_{N0}$ and $\check{\Omega}_F$.

4. Proposed method

4.1. Alarm-range normalization

AR-normalization, as proposed in the preliminary work by Lucke et al. (2018a), uses absolute alarm thresholds of a process variable as a reference for the normalization of the corresponding process measurement. The difference between the high absolute alarm threshold h_m and the low absolute alarm threshold l_m of a process variable X_m can be used to give an indication of the acceptable amplitude of variation of the corresponding process measurement. The AR-normalized plant vector at time t_n is defined as $\tilde{\mathbf{x}}(t_n) = [\tilde{x}_1(t_n), \ \dots \ , \tilde{x}_M(t_n)]^T$ where:

$$\tilde{x}_m(t_n) = \frac{x_m(t_n) - \mu_m(\check{\Omega}_{N0})}{h_m - l_m} \tag{3}$$

4.2. Fault detection and isolation

4.2.1. PCA modeling

The fault detection and isolation in this chapter is based on PCA (MacGregor and Kourti, 1995). PCA is a linear dimensionality reduction technique that

determines the set of orthogonal vectors (called loading vectors) ordered by the amount of variance explained in the loading vectors direction. The PCA model is trained with the training set $\check{\Omega}_{N0}$ of process measurements from normal operation. The $\check{N}$ normalized plant vectors $\tilde{\mathbf{x}}(t_{\check{n}})$ in $\check{\Omega}_{N0}$ are stacked into a matrix $\tilde{\mathbf{X}}_{\check{\mathbf{N}}} \in \mathbb{R}^{\check{N} \times M}$, and the loading vectors are computed via the singular value decomposition (Braatz, L H Chiang and D, 2001):

$$\tilde{\mathbf{X}}_{\check{\mathbf{N}}} = \mathbf{U}\mathbf{\Sigma}\mathbf{V}^T \tag{4}$$

where $\mathbf{U} \in \mathbb{R}^{\check{N} \times \check{N}}$ and $\mathbf{V} \in \mathbb{R}^{M \times M}$ are orthogonal matrices, and the matrix $\mathbf{\Sigma} \in \mathbb{R}^{\check{N} \times M}$ contains the non-negative real singular values λ_m of decreasing magnitude on the diagonal and zero off-diagonal elements.

4.2.2. Fault detection

Each new normalized plant vector $\tilde{\mathbf{x}}(t_n)$ at time t_n is tested with the PCA model to determine if it should be considered as normal or faulty. Hotelling's T^2 statistic and the Q statistic can be used to detect faulty plant vectors (Braatz, L H Chiang and D, 2001). The value of T^2 at time t_n can be computed as:

$$T^2(t_n) = \tilde{\mathbf{x}}(t_n)^T \mathbf{P}{\mathbf{\Sigma}_{\mathbf{M_a}}}^{-2}\mathbf{P}^T\tilde{\mathbf{x}}(t_n) = \tilde{\mathbf{x}}(t_n)^T\mathbf{D}\tilde{\mathbf{x}}(t_n) \tag{5}$$

where $\mathbf{D} = \mathbf{P}{\mathbf{\Sigma}_{\mathbf{M_a}}}^{-2}\mathbf{P}^T$, $\mathbf{\Sigma}_{\mathbf{M_a}}$ contains the first M_a rows and columns of $\mathbf{\Sigma}$ and $\mathbf{P} \in \mathbb{R}^{M \times M_a}$ is the matrix of the loading vectors associated with the M_a largest singular values.

The portion of the observation space corresponding to the $M - M_a$ smallest singular values can be monitored by the Q statistic:

$$Q(t_n) = \mathbf{r}(t_n)^T\mathbf{r}(t_n) = \tilde{\mathbf{x}}(t_n)^T\mathbf{C}\tilde{\mathbf{x}}(t_n) \tag{6}$$

where $\mathbf{r}(t_n) = (\mathbf{I}_M - \mathbf{P}\mathbf{P}^T)\tilde{\mathbf{x}}(t_n)$ is the residual vector at time t_n, $\mathbf{I}_M$ is the identity matrix of size M, and $\mathbf{C} = (\mathbf{I}_M - \mathbf{P}\mathbf{P}^T)$.

$\tilde{\mathbf{x}}(t_n)$ is considered as faulty if $T^2(t_n) \geq T^2_\alpha$ or if $Q(t_n) \geq Q_\alpha$, where T^2_α is the T^2 statistic threshold and Q_α the Q statistic threshold, and α indicates the significance level of the thresholds. T^2_α and Q_α are computed based on

percentiles of the values of T^2 and Q for the process measurements in $\check{\Omega}_{N0}$. In the following, $T^2_{1\%}$ and $Q_{1\%}$ correspond to the thresholds for $\alpha = 1\%$, and $T^2_{0.1\%}$ and $Q_{0.1\%}$ correspond to the thresholds for $\alpha = 0.1\%$.

4.2.3. Fault isolation

If $\tilde{\mathbf{x}}(t_n)$ is detected as faulty, the contribution of each process variable X_m to $T^2(t_n)$ and $Q(t_n)$ is investigated through reconstruction-based contribution analysis Alcala and Qin (2009).The reconstruction-based contribution $f_{T^2,m}(t_n)$ of X_m to $T^2(t_n)$ is:

$$f_{T^2,m}(t_n) = \frac{(\boldsymbol{\xi_m}^T \mathbf{D}\, \tilde{\mathbf{x}}(t_n))^2}{d_{mm}} \tag{7}$$

where $\boldsymbol{\xi_m}$ is the mth column of the m by m identity matrix and d_{mm} is the mth diagonal element of the matrix $\mathbf{D}$ defined in sub-section 4.2.2.

The reconstruction-based contribution $f_{Q,m}(t_n)$ of X_m to $Q(t_n)$ is:

$$f_{Q,m}(t_n) = \frac{r_m^2}{c_{mm}} \tag{8}$$

where r_m is the mth row of the residual vector $\mathbf{r}(t_n)$ and c_{mm} is the mth diagonal element of the matrix $\mathbf{C}$ defined in sub-section 4.2.2.

4.3. Fault identification

If $\tilde{\mathbf{x}}(t_n)$ is detected as faulty, $\tilde{\mathbf{x}}(t_n)$ is compared to normalized plant vectors $\tilde{\mathbf{x}}(t_{\check{n}})$ of the training set of process measurements from faulty operation $\check{\Omega}_F$ to determine if $\tilde{\mathbf{x}}(t_n)$ belongs to one of the fault classes c covered by the classifier. The estimated fault class $\hat{c}(t_n)$ corresponding to $\tilde{\mathbf{x}}(t_n)$ is identified using a popular classifier for fault identification in the industry Vargas et al. (2017), the 1-Nearest Neighbour (1NN) classification algorithm. 1NN associates $\tilde{\mathbf{x}}(t_n)$ with the class $c(t_{\check{n}_1})$ of the nearest neighbour $\tilde{\mathbf{x}}(t_{\check{n}_1})$ of $\tilde{\mathbf{x}}(t_n)$ in $\check{\Omega}_F$:

$$\tilde{\mathbf{x}}(t_{\check{n}_1}) = \underset{\tilde{\mathbf{x}}(t_{\check{n}}) \in \check{\Omega}_F}{\arg\min} \sqrt{\sum_{m=1}^{M} (\tilde{x}_m(t_n) - \tilde{x}_m(t_{\check{n}}))^2} \tag{9}$$

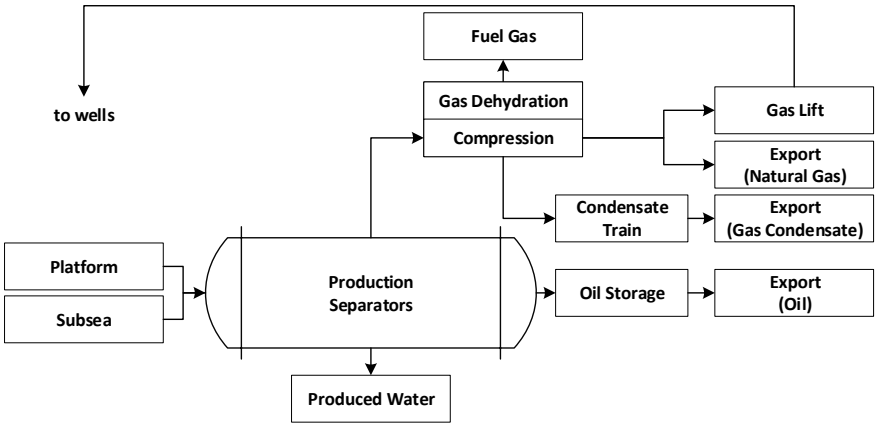

Figure 2: Process overview of the separation plant.

5. Application to industrial case study

5.1. Description of the industrial case study

The industrial case study is an offshore gas oil separation plant, designed to separate crude oil, gas and condensates next to the well before export. An overview of the process is given in Figure 2. The mixture from the well is going through a separation process with two stages of separators. The gas lift and export blocks at the output of the compression block in Figure 2 correspond to natural gas. The output of the condensate train block corresponds to gas condensate, which is a by-product, also exported. The produced water is going through hydrocyclones and then through a degassing drum. A part of the cleaned water is reinjected into the platform through two injection tanks, the Water Injection Tank 1 (WIT1) and the Water Injection Tank 2 (WIT2). The other part of the cleaned water is reversed to the sea. The oil obtained at the output of the hydrocyclones can be reinjected into the second stage of separators, or sent directly to storage facilities after going through the degassing drum.

The study focuses on the Produced Water Reinjection (PWRI) section where the produced water and the produced oil from the hydrocyclones are going

through the degassing drum before being redirected respectively to the injection tanks (or to the sea) and to the oil storage. A detailed diagram of the PWRI section is given in Figure 3. Four pumps ensure the flow of water to the injection tanks. P11 and P12 feed the WIT1, and P21 and P22 feed the WIT2. Another pump ensures the flow of oil from the output of the degassing drum to the oil storage. The level of water in the degassing drum is controlled using several valves. The valve to the WIT1 and the valve to the WIT2 can be closed to ensure a minimum flow going into the degassing drum through the recycle. The valves to the sea can also be opened or closed to regulated the water output.

Recurrent faults have been observed by experts in the PWRI section over a period of four months. Four different types of faults have been labelled and are listed in Table 1:

- Fault 1: the fault starts with a pressure drop in the water coming into the PWRI section, observable through the drop in the suction pressures of P11 and P21. The situation goes back to normal after a few samples.
- Fault 2: the fault is similar to Fault 1 except that the low suction pressure triggers a trip of P21, which means that the situation does not go back to normal as in Fault 1.
- Fault 3: the fault starts with a change in the type of fuel used for the pumps of the PWRI section (from diesel to gas, or vice versa). The fuel change triggers a drop of pressure and flow in the whole water system that can lead to a trip of P11 or P21 (or both).
- Fault 4: the fault starts with a trip of P21 due to high vibrations in the motor of the pump.

Table 2 lists the 16 process variables measured in the PWRI section with a sampling time of one second. For each process variable, the table indicates the high and low alarm thresholds defined in the alarm system, as well as the alarm range. The table also indicates the standard deviation of each process variable in fault-free operation and during the selected faults.

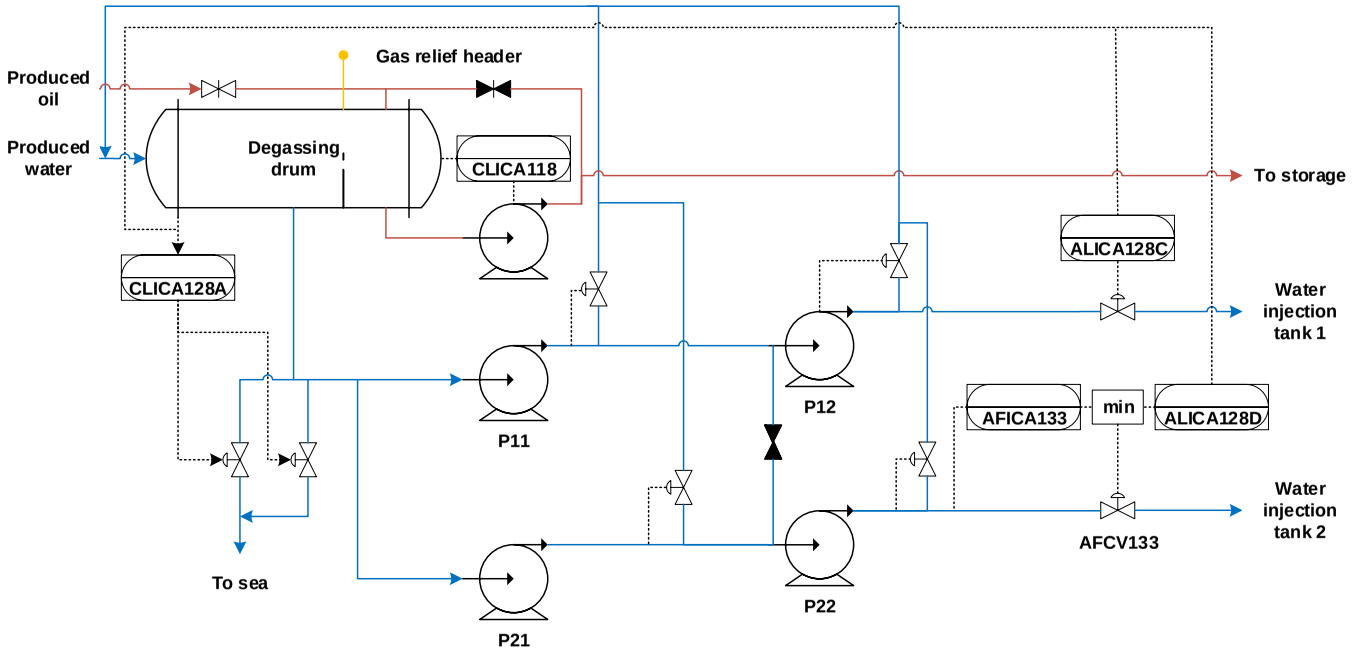

Figure 3: Process diagram of the PWRI section that deals with the produced water of Figure 2. Blue indicates the water system, brown the oil system, and yellow the gas system.

Table 1: Selected faults in the PWRI section.

Fault	Description	Number of occurrences
1	Low suction pressure without pump trip	2
2	Low suction pressure with P21 trip	3
3	Fuel change	8
4	P21 trip due to vibrations	2

5.2. Design of experiment

AR-normalization is compared to N-standardization for fault detection and isolation, and AR-normalization is compared to F-standardization for fault identification. N-standardization uses the standard deviation $\sigma_m(\check{\Omega}_{N0})$ computed on the training set of process measurements from normal operation $\check{\Omega}_{N0}$, while F-standardization uses the standard deviation $\sigma_m(\check{\Omega}_F)$ computed on the training set of process measurements from faulty operation $\check{\Omega}_F$. AR-normalization uses the difference between the high alarm threshold h_m and the low alarm threshold l_m. All three normalizations use the mean $\mu_m(\check{\Omega}_{N0})$ computed during normal operation.

5.2.1. Fault detection and isolation

Figure 4 represents the N-standardized process measurements and the AR-normalized process measurements during normal operation in the training set $\check{\Omega}_{N0}$. The values of $\sigma_m(\check{\Omega}_{N0})$ for each process variable are indicated in Table 2.

A PCA model is built on the N-standardized measurements and another PCA model is built for the AR-normalized measurements. APZT141 is not included in the PCA model since it does not move during normal operation. The number of loading vectors is set to 10 (i.e. $M_a = 10$).

Table 2: Process variables

Original tag	Description	Unit	l_m	h_m	$h_m - l_m$	$\sigma_m(\check{\Omega}_{N0})$	$\sigma_m(\check{\Omega}_F)$
CLY128A	Water level degassing drum	%	0.00	90.00	90.00	1.04	11.34
CPZT151	Suction pressure P11	barg	0.40	7.00	6.60	0.02	0.26
CPZT112	Suction pressure P21	barg	0.60	7.00	6.40	0.01	0.31
AFT121	Water flow to WIT2	m3/h	250.00	900.00	650.00	1.75	344.85
AFZT114	Inlet flow P22	Sm3/h	470.00	900.00	430.00	2.07	278.77
AFZT139	Water flow to WIT2	m3/h	200.00	900.00	700.00	1.96	290.08
AFZT115	Discharge flow P21	m3/h	340.00	750.00	410.00	3.46	285.05
ALT148	Water level of the injection rundown tank	%	10.00	95.00	85.00	0.10	0.08
APT123	Suction pressure P12 and P22	barg	7.10	40.00	32.90	0.01	3.73
APT146	Discharge pressure P22	barg	90.00	193.00	103.00	0.10	57.36
APZT141	Discharge pressure P11	barg	10.00	23.00	13.00	0.00	7.57
APZT154	Suction pressure P12	barg	6.50	23.00	16.50	0.01	1.24
APZT143	Discharge pressure P12	barg	8.00	170.00	162.00	0.09	14.13
APZT117	Discharge pressure P21	barg	10.00	23.00	13.00	0.02	12.37
APZT140	Suction pressure P22	barg	6.50	23.00	16.50	0.02	3.67
APZT142	Discharge pressure P22	barg	85.00	215.00	130.00	0.05	59.64

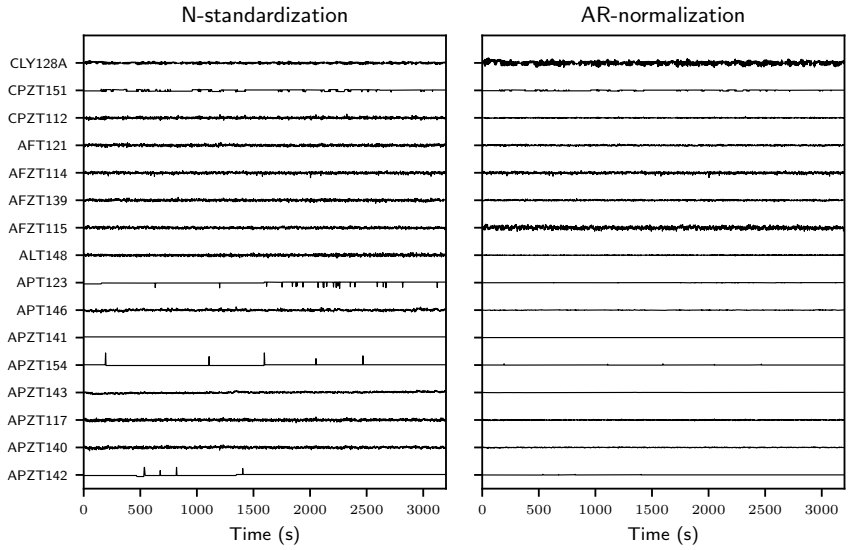

Figure 4: Process measurements in the training set $\check{\Omega}_{N0}$ normalized with N-standardization and AR-normalization. The scale is $[-20, 20]$ for each N-standardized measurement and $[-0.1, 0.1]$ for each AR-normalized measurement.

The fault detection is done on a test set of measurements from normal operation Ω_{N0}. The training set $\check{\Omega}_F$ used for training the fault identification model is also used for testing the detection and isolation on one occurrence of each type of fault. The reconstruction-based contribution plots for T^2 and Q are analysed for each of those faults.

5.2.2. Fault identification

The training set $\check{\Omega}_F$ containing one occurrence of each type of fault listed in Table 1 is used for training the classifier for the fault identification. Figure 5 represents the normalized process measurements during each type of fault in $\check{\Omega}_F$. The blue dotted lines correspond to the F-standardized measurements, and the red lines correspond to the AR-normalized measurements. The values of $\sigma_m(\check{\Omega}_F)$ for each process variable are indicated in Table 2.

The classifier is tested on a test set of data from the remaining fault occurrences, Ω_F. The new fault occurrences are detected using the PCA model with

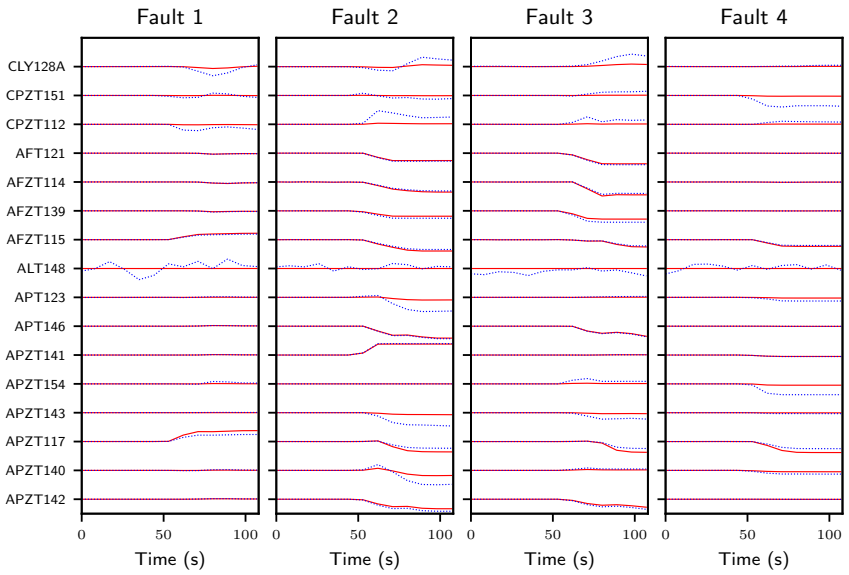

Figure 5: Process measurements in the training set $\check{\Omega}_F$ normalized with F-standardization (blue) and AR-normalization (red). The scale is $[-4, 4]$ for each F-standardized measurement and $[-2, 2]$ for each AR-normalized measurement.

AR-normalization, and a classification is proposed for each sample as soon as the fault is detected. The fault identification focuses on the four types of faults of Table 1 and does not consider unknown types of faults.

6. Results

6.1. PCA modeling

Figure 6 indicates the cumulative variance explained by the loading vectors of the PCA with N-standardization (in blue) and with AR-normalization (in red). The slope is steeper for AR-normalization than for N-standardization. This shows that the variance explained by the loading vectors associated to the largest singular values is larger for AR-normalization than for N-standardization, and that the variance explained by the loading vectors associated to the smallest singular values is negligible for AR-normalization.

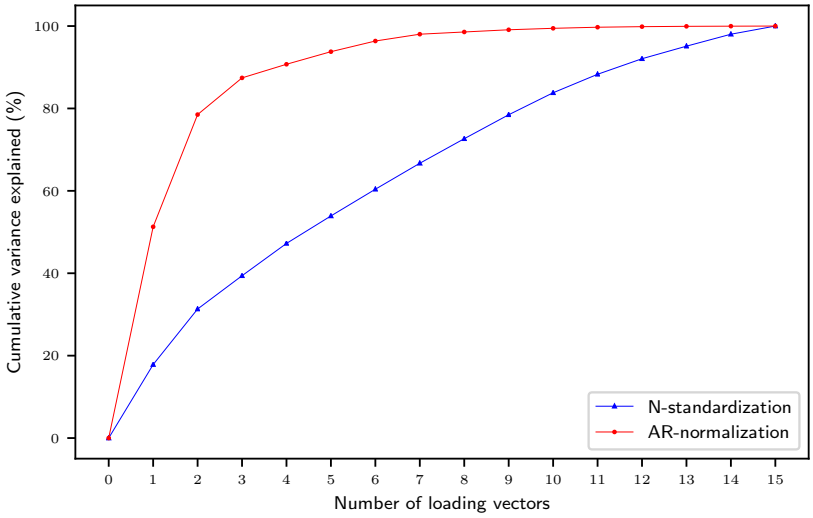

Figure 6: Cumulative variance explained by the loading vectors on $\check{\Omega}_{N0}$ with N-standardization and AR-normalization.

The PCA model with AR-normalization emphasizes the variations that are the most representative compared to the safe operation range defined by the alarm thresholds. This has two benefits. The first benefit is to build a model capturing the representative variations and limiting the impact of small variations (compared to the alarm thresholds) that may not give a good indication of the variability of the measurements in the normal operation data available for training. The second benefit is to give more weight to process measurements with larger variations compared to their alarm threshold, since those process measurements are the most likely to reach their alarm thresholds. Therefore, each variation of those variations should have a high impact on the detection statistic T^2.

Capturing small variations in the model can have a negative impact. N-standardization gives the same weight to all process measurements in $\check{\Omega}_{N0}$ since they are all scaled to unit-variance. Process measurements with small variations in $\check{\Omega}_{N0}$ have the same weight as the other ones, even though the variations

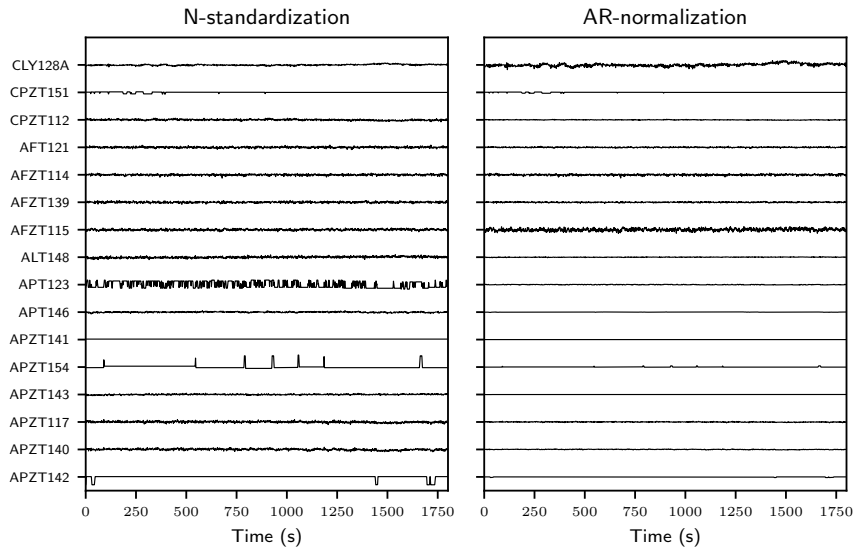

Figure 7: Process measurements in the test set Ω_{N0} normalized with N-standardization and AR-normalization. The scale is $[-20, 20]$ for each N-standardized measurement and $[-0.1, 0.1]$ for each AR-normalized measurement.

may only represent minor fluctuations. Therefore, any move of one of those process measurements has a major impact on the detection statistic T^2. This can trigger false detections and can introduce a bias in the contribution plots when it comes to fault isolation. Not monitoring the process measurements with small variations can lead to missed detections, but those process measurements do not need to be included in the PCA model and can be monitored by the Q statistic.

6.2. Fault detection

The fault detection is tested on a test set of data from normal process operation Ω_{N0}, plotted in Figure 7. The values of the T^2 statistic are plotted in Figure 8 for N-standardization and AR-normalization, and the values of the Q statistic are plotted in Figure 9 for N-standardization and AR-normalization. For each plot, two detection thresholds are represented, for $\alpha = 1\%$ and for $\alpha = 0.1\%$. Table 3 shows the false detection rates for each normalization approach with

Table 3: False detection rates on the test set Ω_{N0} with N-standardization and AR-normalization.

	T^2		Q		T^2 OR Q	
α	1%	0.1%	1%	0.1%	1%	0.1%
N-standardization	0.058	0.007	0.111	0.012	0.118	0.019
AR-normalization	0.003	0.000	0.067	0.012	0.070	0.012

T^2, with Q, and with T^2 OR Q where a plant vector is detected as faulty if it is faulty with T^2 or with Q. The false detection rate is expressed as the ratio of plant vectors in the test set Ω_{N0} detected as faulty compared to the total number of plant vectors in Ω_{N0}. The false detection rates are given for the detection thresholds with $\alpha = 1\%$ and for the detection thresholds with $\alpha = 0.1\%$. $T^2_{0.1\%}$ and $Q_{0.1\%}$ are retained for the rest of the chapter as they provide a better robustness with regard to fault detection for both N-standardization and AR-normalization.

The false detection rates for T^2 with AR-normalization are much lower than the false detection rates for T^2 with N-standardization. For exampled, the T^2 statistic with N-standardization in Figure 8 presents a series of spikes that lead to false detections. Those spikes corresponds to small variations in APZT154 and APZT142 that had a small variability in the training set $\check{\Omega}_{N0}$. The T^2 statistic with AR-normalization is more robust as it does not depend as much on those process measurements.

Some of the variations in APZT154 and APZT142 are captured by the Q statistic with AR-normalization, but the impact is not as high as with N-standardization since the false detection rates for Q are still smaller with AR-normalization than with N-standardization (Table 3). Generally speaking, the false detection rates with T^2 OR Q indicate that the fault detection is more robust with AR-normalization than with N-standardization.

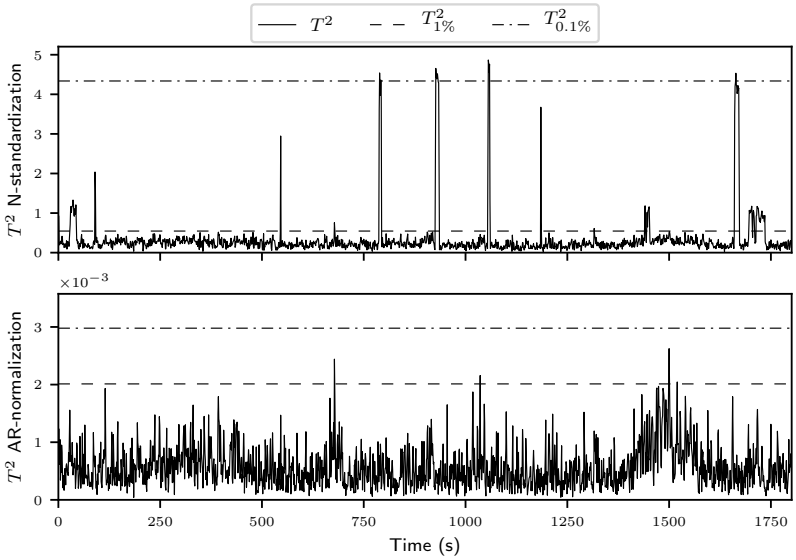

Figure 8: T^2 statistic for the test set Ω_{N0} with N-standardization (top) and AR-normalization (bottom).

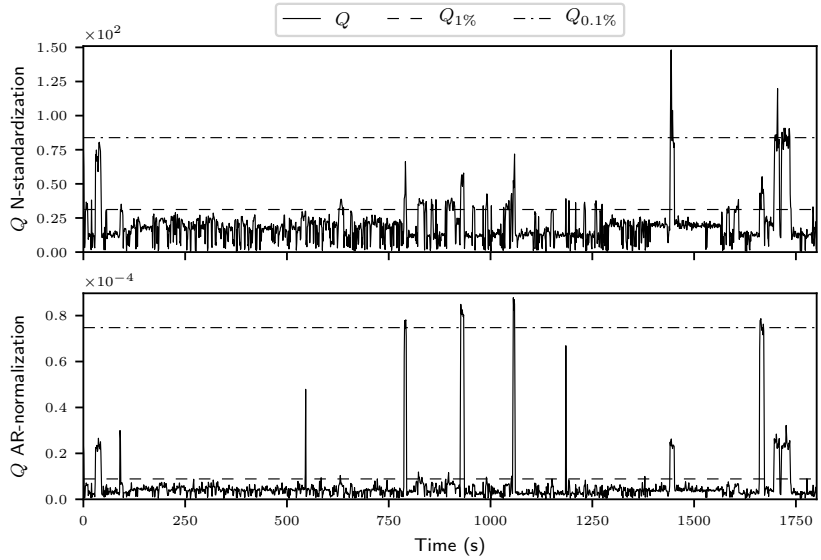

Figure 9: Q statistic for the test set Ω_{N0} with N-standardization (top) and AR-normalization (bottom).

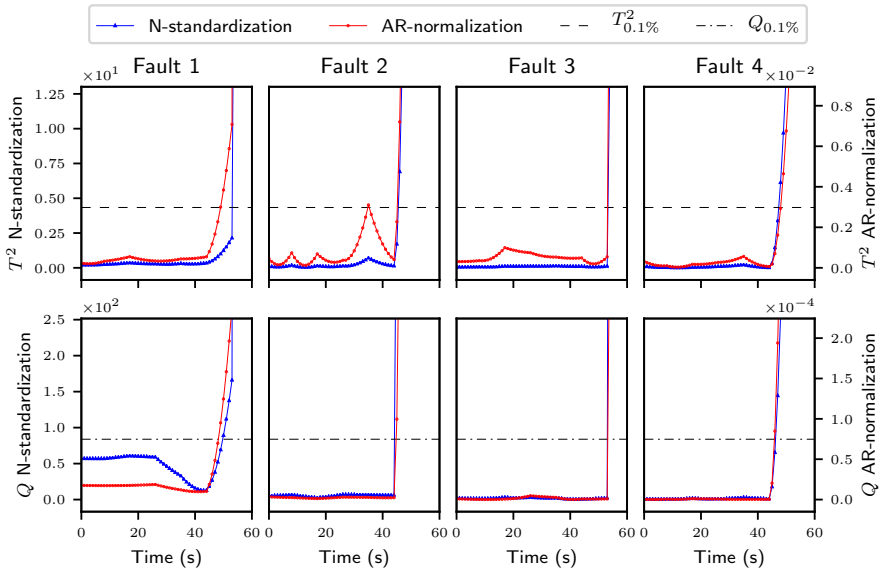

Figure 10: T^2 and Q statistics with N-standardization (blue) and with AR-normalization (red) for one occurrence of each type of fault in $\check{\Omega}_F$.

Figure 10 shows the T^2 and Q statistics for one occurrence of each fault with the corresponding detection thresholds $T^2_{0.1\%}$ and $Q_{0.1\%}$. The blue lines correspond to the scores with N-standardization, the red lines correspond to the scores with AR-normalization. All four faults are well detected with T^2 and Q for both N-standardization and AR-normalization, although AR-normalization offers a better detection performance than N-standardization, in particular for Fault 1. The deviation in the discharge pressure of P21 (APZT117) that occurs in Fault 1 is given more abnormal compared to the alarm range than compared to the standard deviation in in training set, and T^2 with AR-normalization detects the fault before T^2 with N-standardization.

6.3. Fault isolation

Figure 11 shows the T^2 reconstruction-based contributions with N-standardization (in blue) and with AR-normalization (in red) for one occurrence of each type of fault, and Figure 12 shows the Q reconstruction-based contributions with N-

standardization (in blue) and with AR-normalization (in red). The reconstruction-based contributions are plotted in the early stage of the fault, as soon as it is detected, to identify the first variables affected.

For the first three faults, the T^2 reconstruction-based contribution plots with N-standardization and with AR-normalization are comparable. APZT117 (discharge pressure of P21) and APZT140 (suction pressure of P22) are identified as the most contributing variables in Fault 1 since the pressure drop in the incoming water has more effect on P21 than on P11. The pressure drop in the incoming water also affects APZT117 and APZT140 in Fault 2 but the trip of P21 has an immediate effect on the discharge pressures of P22 (APZT142) and P12 (APZT143), whose T^2 contributions exceed the ones of APZT117 and APZT140. For Fault 3, N-standardization and AR-normalization both highlight the T^2 contribution of AFZT139, the water flow to the water injection tank WIT2. While the whole water system is affected by the drop in pressure and flow caused by the fuel change, the effect on AFZT139 has more importance because the water flow to WIT2 is the key controlled variable of the system. Any variation in this flow is considered as highly abnormal, both compared to statistical variations in the training set $\check{\Omega}_{N0}$ and compared to the alarm thresholds.

However, the T^2 contributions with N-standardization and with AR-normalization differ for Fault 4. APZT154 (suction pressure of P12) is identified as the most contributing variable to Fault 4 with N-standardization but has a minor T^2 contribution with AR-normalization. This is because APZT154 presents small variations in the training set $\check{\Omega}_{N0}$. The high contribution of this variable hides the real root cause of the fault. Fault 4 starts with a trip of P21 (due to high vibrations in the motor of the pump), so the process variables affiliated to this pump should be highlighted as root causes. The highest contribution to the T^2 statistic with AR-normalization for this fault is APZT117 which is the discharge pressure of P21. Therefore, Fault 4 is an example of how AR-normalization improves the fault isolation by highlighting in priority the process measurements with large variations compared to their alarm thresholds.

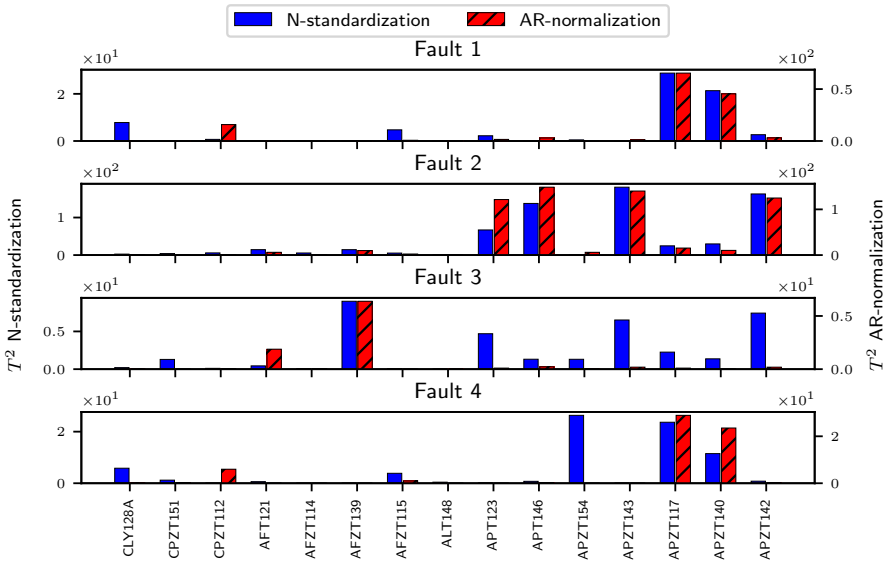

Figure 11: T^2 reconstruction-based contribution plots with N-standardization (blue) and with AR-normalization (red) for one occurrence of each type of fault in $\check{\Omega}_F$.

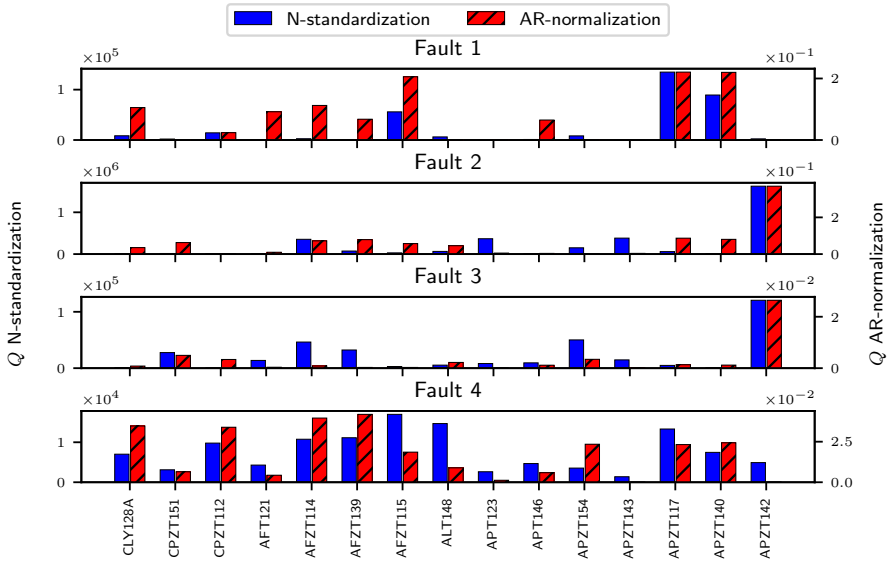

Figure 12: Q reconstruction-based contribution plots with N-standardization (blue) and with AR-normalization (red) for one occurrence of each type of fault in $\check{\Omega}_F$.

The Q contributions of Figure 12 confirm some of the variables isolated using the T^2 contributions (e.g. APZT117 and APZT140 for Fault 1 and Fault 4 and APZT142 for Fault 2) and highlight some variables that are not captured in T^2 such as the discharge flow of P21 (AFZT115) in Fault 1.

6.4. Fault identification

The fault identification is tested on a test set Ω_F of data containing new occurrences of faults 1 to 4. Figure 13 and Figure 14 show the classification results respectively with F-standardization and AR-normalization. The classification results are displayed for each fault occurrence, and Fault 2-1 and Fault 2-2 correspond for example to the first and second occurrences of Fault 2 in Ω_F. For each figure, the detection is done using the T^2 statistic of the PCA with AR-normalization. The classification outcome is displayed as soon as the fault is detected. Each point indicates a new sample appearing every second. Black points indicate samples that are not detected as faulty, and the other colours indicate the classification outcome.

Classification with AR-normalization outperforms classification with F-standardization in both early stage classification and steady-state classification. For early stage classification, the classifier with AR-normalization correctly identifies faults 2-1, 2-2, 3-1, 3-2, 3-4, 3-6 and 4-1 before the classifier with F-standardization. For steady-state classification, the classifier with AR-normalization identifies all faults correctly in their steady-state while the classifier with F-standardization classifies Fault 2-1 as Fault 3 and Fault 3-7 as Fault 2.

Fault 3-7 illustrates the advantages of AR-normalizations over F-standardization. This occurrence of Fault 3 is classified as Fault 2 in steady-state with F-standardization, but is correctly classified with AR-normalization. Figure 15 gives more details about the classification for this fault. The figure shows the values taken by each process variable during the training occurrence of Fault 2 (in yellow) and during the training occurrence of Fault 3 (in green), as well as the values taken during Fault 3-7 (in red). The values are displayed for F-standardization and AR-normalization. The mean-centered values are also displayed for comparison.

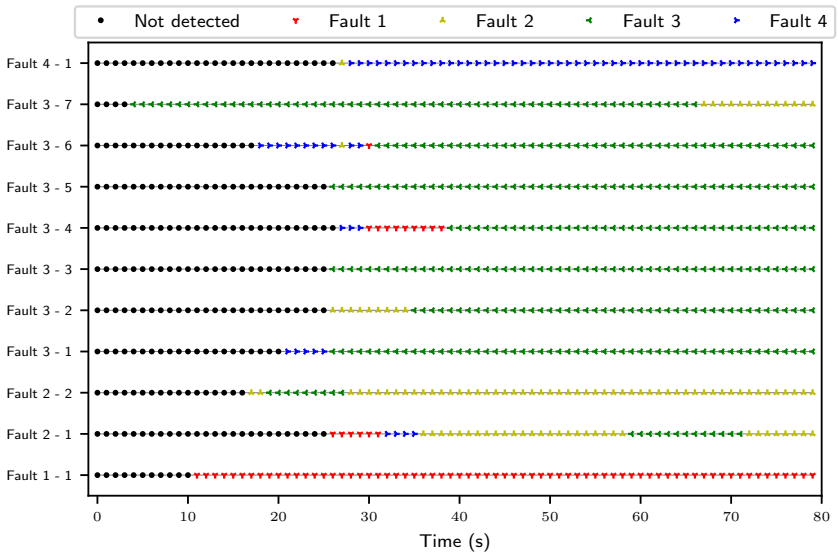

Figure 13: Classification outcomes with 1NN and F-standardization.

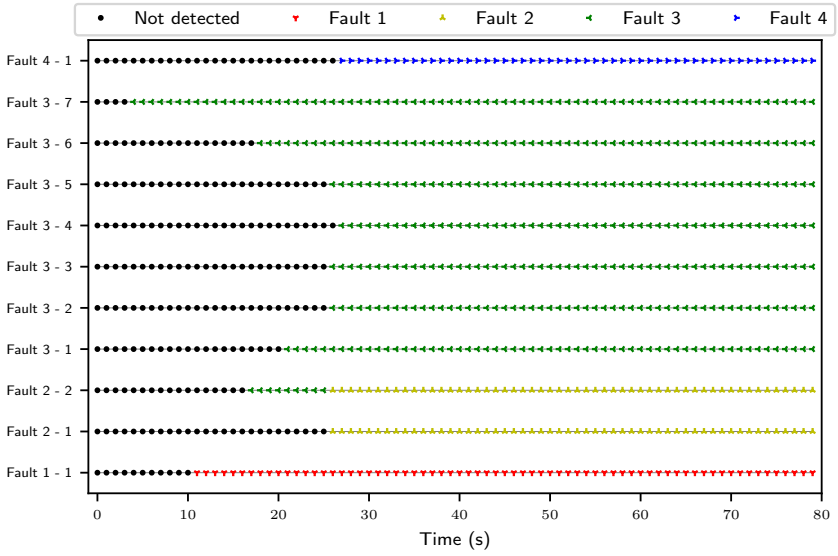

Figure 14: Classification outcomes with 1NN and AR-normalization.

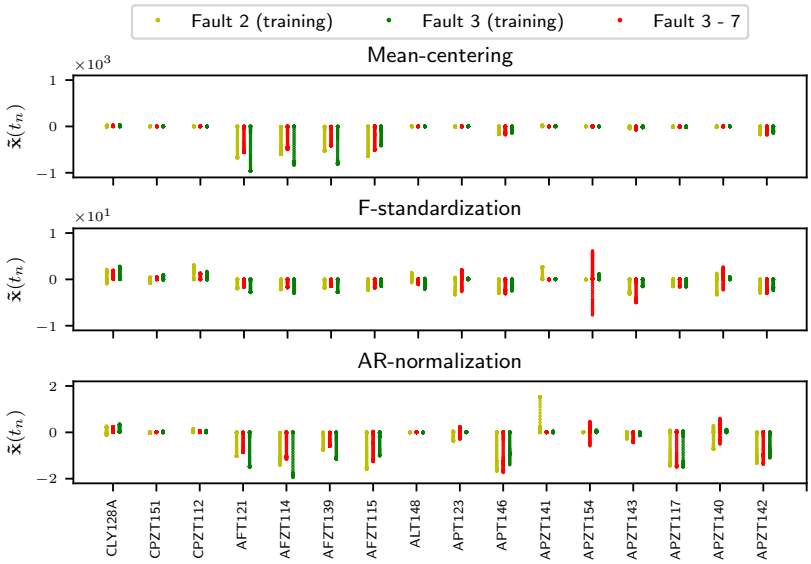

Figure 15: Normalized plant vectors $\tilde{\mathbf{x}}(t_n)$ for the training occurrence of Fault 2 (yellow) and Fault 3 (green), and for Fault 3-7 (red). Each point corresponds to the value of each process variable in $\tilde{\mathbf{x}}(t_n)$ at a certain time t_n during the development of the fault.

The main discriminating process variable between Fault 2 and Fault 3 is APZT141, which is the discharge pressure of P11. In the case of Fault 2, APZT141 increases significantly since the trip of P21 causes P11 to pump more water. In Fault 3, all the pumps of the PWRI section are affected by the fuel change and the flow and pressure in the water system go down. In this case, the discharge pressure of P11 stays constant or decreases.

With mean-centering or F-standardization, the variations of APZT141 are small compared to the variations of other process variables. AR-normalization shows that the variations of APZT141 are actually significant (in Fault 2) compared to its alarm thresholds, and the weight of the variations of other process variables is reduced. As a result, the behaviour of APZT141 has a major impact on the classification outcome with AR-normalization, and Fault 3-7 is correctly classified. With the other normalizations, Fault 3-7 is misclassified as Fault 2 since the amplitudes of the drop in the flows (AFT121, AFZT114, AFZT139,

and AFZT115) are closer to the amplitude of the drops in Fault 2 than in Fault 3.

7. Conclusion

Recent work has demonstrated the benefits of integrating alarm logs in fault detection and diagnosis. This paper affirms that alarm settings defined during the alarm design stage based on engineering and safety considerations can also be exploited to improve fault detection, fault isolation and fault identification. A normalization of the process measurements based on their alarm thresholds is proposed. Fault detection and diagnosis methods are dependent on the availability of process measurements, and the current normalization methods such as standardization are also impacted by the choice of the training set. AR-normalization is independent of the statistics of the training data and takes into account the acceptable range of variation of each process measurement. The oil gas separation plant case study showed how traditional standardization approaches could lead to spurious results when some process measurements in the training data do not present representative variations. In this case, AR-normalization improved the robustness of the fault detection, isolation, and identification.

8. Conflict of interest

The authors declare that there is no conflict of interest in this paper.

References

Alcala, C.F., Qin, S.J., 2009. Reconstruction-based contribution for process monitoring. Automatica 45, 1593–1600. doi:10.1016/j.automatica.2009.02.027.

Braatz, L H Chiang, E.L.R., D, R., 2001. Fault Detection and Diagnosis in Industrial Systems. Advanced Textbooks in Control and Signal Processing, Springer London, London. doi:10.1088/0957-0233/12/10/706.

Charbonnier, S., Bouchair, N., Gayet, P., 2015. A weighted dissimilarity index to isolate faults during alarm floods. Control Engineering Practice 45, 110–122. doi:10.1016/j.conengprac.2015.09.004.

Charbonnier, S., Bouchair, N., Gayet, P., 2016. Fault template extraction to assist operators during industrial alarm floods. Engineering Applications of Artificial Intelligence 50, 32–44. doi:10.1016/j.engappai.2015.12.007.

Dorgo, G., Pigler, P., Abonyi, J., 2018. Understanding the importance of process alarms based on the analysis of deep recurrent neural networks trained for fault isolation. Journal of Chemometrics , 1–18doi:10.1002/cem.3006.

Gajjar, S., Palazoglu, A., 2016. A data-driven multidimensional visualization technique for process fault detection and diagnosis. Chemometrics and Intelligent Laboratory Systems 154, 122–136. doi:10.1016/j.chemolab.2016.03.027.

Ge, Z., Song, Z., Ding, S.X., Huang, B., 2017. Data mining and analytics in the process industry: The role of machine learning. IEEE Access 5, 20590–20616. doi:10.1109/ACCESS.2017.2756872.

Ge, Z., Song, Z., Gao, F., 2013. Review of recent research on data-based process monitoring. Industrial and Engineering Chemistry Research 52, 3543–3562. doi:10.1021/ie302069q.

Hollifield, B.R., Habibi, E., 2011. Alarm Management: A Comprehensive Guide: Practical and Proven Methods to Optimize the Performance of Alarm Management Systems. ISA.

Hu, W., Chen, T., Shah, S.L., Hollender, M., 2017a. Cause and effect analysis for decision support in alarm floods. IFAC-PapersOnLine 50, 13940–13945. doi:10.1016/j.ifacol.2017.08.2215.

Hu, W., Wang, J., Chen, T., Shah, S.L., 2017b. Cause-effect analysis of industrial alarm variables using transfer entropies. Control Engineering Practice 64, 205–214. doi:10.1016/j.conengprac.2017.04.012.

IEC (International Electrotechnical Commission), 2014. Management of Alarm Systems for the Process Industries. IEC 62682. IEC.

Lai, S., Yang, F., Chen, T., 2017. Online pattern matching and prediction of incoming alarm floods. Journal of Process Control 56, 69–78. doi:10.1016/j.jprocont.2017.01.003.

Lucke, M., Chioua, M., Grimholt, C., Hollender, M., Thornhill, N.F., 2018a. On improving fault detection and diagnosis using alarm-range normalisation, in: Proceedings of 10th SAFEPROCESS Symposium, Warsaw, Poland, August 29-31, IFAC-PapersOnLine, pp. 1227–1232. doi:10.1016/j.ifacol.2018.09.695.

Lucke, M., Chioua, M., Grimholt, C., Hollender, M., Thornhill, N.F., 2018b. Online alarm flood classification using alarm coactivations, in: Proceedings of 10th ADCHEM Symposium, Shenyang, China, July 25-27, IFAC-PapersOnLine, pp. 345–350. doi:10.1016/j.ifacol.2018.09.324.

Lucke, M., Chioua, M., Grimholt, C., Hollender, M., Thornhill, N.F., 2019a. Advances in alarm data analysis with a practical application to online alarm flood classification. Journal of Process Control 79, 56–71. doi:10.1016/j.jprocont.2019.04.010.

Lucke, M., Mei, X., Stief, A., Chioua, M., Thornhill, N.F., 2019b. Variable selection for fault detection and identification based on mutual information of alarm series, in: Proceedings of 12th DYCOPS Symposium, Florianópolis, Brazil, April 23 - 26, IFAC-PapersOnLine, pp. 673–678. doi:10.1016/j.ifacol.2019.06.140.

MacGregor, J.F., Kourti, T., 1995. Statistical process control of multivariate processes. Control Engineering Practice 3, 403–414. doi:10.1016/0967-0661(95)00014-L.

Rodrigo, V., Chioua, M., Hagglund, T., Hollender, M., 2016. Causal analysis for alarm flood reduction. Proceedings of 11th DYCOPS Symposium, Trondheim,

Norway, June 6-8, 2016, IFAC-PapersOnLine 49, 723–728. doi:10.1016/j.ifacol.2016.07.269.

Shang, J., Chen, M., Ji, H., Zhou, D., 2017a. Recursive transformed component statistical analysis for incipient fault detection. Automatica 80, 313–327. doi:10.1016/j.automatica.2017.02.028.

Shang, J., Chen, M., Ji, H., Zhou, D., Zhang, H., Li, M., 2017b. Dominant trend based logistic regression for fault diagnosis in nonstationary processes. Control Engineering Practice 66, 156–168. doi:10.1016/j.conengprac.2017.06.011.

Shu, Y., Zhao, J., 2016. Fault diagnosis of chemical processes using artificial immune system with vaccine transplant. Industrial and Engineering Chemistry Research 55, 3360–3371. doi:10.1021/acs.iecr.5b02646.

Stief, A., Ottewill, J.R., Tan, R., Cao, Y., 2018. Process and alarm data integration under a two-stage Bayesian framework for fault diagnostics. IFAC-PapersOnLine 51, 1220–1226. doi:10.1016/j.ifacol.2018.09.696.

Stief, A., Tan, R., Cao, Y., Ottewill, J.R., Thornhill, N.F., Baranowski, J., 2019. A heterogeneous benchmark dataset for data analytics: Multiphase flow facility case study. Journal of Process Control 79, 41–55. doi:10.1016/j.jprocont.2019.04.009.

Su, J., Wang, D., Zhang, Y., Yang, F., Zhao, Y., Pang, X., 2017. Capturing causality for fault diagnosis based on multi-valued alarm series using transfer entropy. Entropy 19, 663. doi:10.3390/e19120663.

Tong, C., Palazoglu, A., 2016. Dissimilarity-based fault diagnosis through ensemble filtering of informative variables. Industrial and Engineering Chemistry Research 55, 8774–8783. doi:10.1021/acs.iecr.6b00915.

Vargas, R.E., Munaro, C.J., Ciarelli, P.M., De Araujo, J.C., 2017. Proposal for two classifiers of offshore naturally flowing wells events using k-nearest neighbors, sliding windows and time multiscale, in: 2017 6th International

Symposium on Advanced Control of Industrial Processes, AdCONIP 2017, IEEE. pp. 209–214. doi:10.1109/ADCONIP.2017.7983782.

Wang, J., Yang, F., Chen, T., Shah, S.L., 2016. An overview of industrial alarm systems: Main causes for alarm overloading, research status, and open problems. IEEE Transactions on Automation Science and Engineering 13, 1045–1061. doi:10.1109/TASE.2015.2464234.

Wu, H., Zhao, J., 2018. Deep convolutional neural network model based chemical process fault diagnosis. Computers and Chemical Engineering 115, 185–197. doi:10.1016/j.compchemeng.2018.04.009.

Xu, J., Wang, J., Izadi, I., Chen, T., 2012. Performance assessment and design for univariate alarm systems based on FAR, MAR, and AAD. IEEE Transactions on Automation Science and Engineering 9, 296–307. doi:10.1109/TASE.2011.2176490.

Yang, F., Guo, C., 2017. Survey on advanced alarm strategies based on multivariate analysis, in: 2017 6th International Symposium on Advanced Control of Industrial Processes, AdCONIP 2017, IEEE. pp. 612–617. doi:10.1109/ADCONIP.2017.7983850.

Yu, W., Yang, F., 2015. Detection of causality between process variables based on industrial alarm data using transfer entropy. Entropy 17, 5868–5887. doi:10.3390/e17085868.

Zhang, Z., Zhao, J., 2017. A deep belief network based fault diagnosis model for complex chemical processes. Computers and Chemical Engineering 107, 395–407. doi:10.1016/j.compchemeng.2017.02.041.

Zhu, Z.B., Song, Z.H., 2010. Fault diagnosis based on imbalance modified kernel Fisher discriminant analysis. Chemical Engineering Research and Design 88, 936–951. doi:10.1016/j.cherd.2010.01.005.